Title
Complex Magnetic Ordering in Eu3InP3: A New Rare Earth Metal Zintl Compound

Journal
Inorganic Chemistry, 44(7)

ISSN
0020-1669

Authors
Jiang, Jiong
Payne, Amy C
Olmstead, Marilyn M
et al.

Publication Date
2005-04-01

DOI
10.1021/ic048507o

Inorg. Chem. **2005**, *44*, 2189–2197

Complex Magnetic Ordering in Eu_3InP_3: A New Rare Earth Metal Zintl Compound

Jiong Jiang, Amy C. Payne, Marilyn M. Olmstead, Han-oh Lee,† Peter Klavins,† Zachary Fisk,† and Susan M. Kauzlarich*

Departments of Chemistry and Physics, University of California—Davis, One Shields Avenue, Davis, California 95616

Raphaël P. Hermann and Fernande Grandjean

Department of Physics, B5, University of Liège, B-4000 Sart-Tilman, Belgium

Gary J. Long

Department of Chemistry, University of Missouri—Rolla, Rolla, Missouri 65409-0010

Received October 25, 2004

Eu_3InP_3 has been prepared as large single crystals with an indium flux reaction. The structure of the new compound is isotypic to Sr_3InP_3 and crystallizes in the orthorhombic space group *Pnma* with unit cell dimensions of $a = 12.6517(15)$ Å, $b = 4.2683(5)$ Å, and $c = 13.5643(14)$ Å ($Z = 4$, $T = 140$ K, R1 = 0.0404, wR2 = 0.0971 for all data). The structure consists of one-dimensional chains of corner-shared distorted $[InP_2P_{2/2}]^{6-}$ tetrahedra separated by rows of Eu^{2+} ions. Two of the three crystallographically distinct europium sites have a short Eu(1)–Eu(2) distance of 3.5954(7) Å, which yields Eu–Eu dimers. The Eu–P bond distances range from 2.974(2) to 3.166(2) Å. The temperature dependence of the conductivity indicates that Eu_3InP_3 is a small band gap semiconductor. Both magnetization and Eu-151 Mössbauer spectral measurements indicate that the europium in Eu_3InP_3 is divalent and that at least two magnetic transitions occur. Magnetization studies reveal magnetic transitions at 14, 10.4, and ~5 K. These transitions are also observed in heat capacity studies of Eu_3InP_3. The Mössbauer spectra indicate that the two europium sites are ordered at 12 K and that all three europium sites are ordered at 8 K.

Introduction

Zintl phases are valence-specific compounds formed between electropositive elements, such as alkali metal, alkaline earth metal, and, more recently, rare earth elements, and the main group elements.[1−4] There are a significant number of Zintl compounds composed of the alkali or alkaline earth metals and the elements of groups 13−16. Although there is less known about the rare earth compounds, there has been a recent flurry of research[5] on them because of their promising thermoelectric properties.[6−13] In addition, superconductivity has been discovered in several Zintl compounds.[5,13−15] Because of their unique magnetoresistive properties,[16−22] we have been exploring a flux synthesis

* Author to whom correspondence should be addressed. E-mail: smkauzlarich@ucdavis.edu.
† Department of Physics, University of California—Davis.

(1) Schäfer, H.; Eisenmann, B.; Müller, W. *Angew. Chem., Int. Ed. Engl.* **1973**, *12*, 694−712.
(2) Schäfer, H.; Eisenmann, B. *Rev. Inorg. Chem.* **1981**, *3*, 29−101.
(3) Schäfer, H. *Annu. Rev. Mater. Sci.* **1985**, *15*, 1−41.
(4) Kauzlarich, S. M. *Chemistry, Structure, and Bonding of Zintl Phases and Ions*; VCH Publishers: New York, 1996; p 306.
(5) Mills, A. M.; Lam, R.; Ferguson, M. J.; Deakin, L.; Mar, A. *Coord. Chem. Rev.* **2002**, *233−234*, 207−222.
(6) Mahan, G.; Sales, B.; Sharp, J. *Phys. Today* **1997**, *50*, 42−47.
(7) Ferguson, M. J.; Ellenwood, R. E.; Mar, A. *Inorg. Chem.* **1999**, *38*, 4503−4509.
(8) Chung, D.-Y.; Hogan, T.; Brazis, P.; Rocci-Lane, M.; Kannewurf, C.; Bastea, M.; Uher, C.; Kanatzidis, M. G. *Science* **2000**, *287*, 1024−1027.
(9) Kim, S.-J.; Hu, S.; Uher, C.; Kanatzidis, M. G. *Chem. Mater.* **1999**, *11*, 3154−3159.
(10) Kim, S.-J.; Ireland, J. R.; Kannewurf, C.; Kanatzidis, M. G. *J. Solid State Chem.* **2000**, *155*, 55−61.
(11) Mao, J.; Guloy, A. M. *J. Alloys Compd.* **2001**, *322*, 135−142.
(12) Kim, S.-J.; Salvador, J.; Bilc, D.; Mahanti, S. D.; Kanatzidis, M. G. *J. Am. Chem. Soc.* **2001**, *123*, 12704−12705.
(13) Mills, A. M.; Deakin, L.; Mar, A. *Chem. Mater.* **2001**, *13*, 1778−1788.

10.1021/ic048507o CCC: $30.25
Published on Web 02/23/2005

technique for growing large crystals of the $Ln_{14}MnPn_{11}$ compounds, where Ln is Eu or Yb and Pn is P, As, Sb, or Bi. This research effort has led to the discovery of several new compounds with unique magnetic and electronic properties.[23−25]

Several ternary, europium-containing transition metal pnictides have been discovered that have unusual magnetic properties. $EuNi_5P_3$ has a series of steps in its magnetization curve[26] that result from a magnetic spin-flip transition in combination with thermally activated domain wall motion. A small Eu−Eu distance of 3.62 Å along the *a*-axis is believed to be responsible for the strong magnetic interactions observed[26] in $EuNi_5P_3$. $EuAs_3$ exhibits similar steps in its magnetization curve, and its magnetic phase diagram has been studied[27−30] by several groups; the temperature and field dependences of the lattice parameters are believed to be important in producing the steps in the magnetization.[31]

Europium-containing Zintl phases,[32,33] such as $Eu_{14}InSb_{11}$ and EuZnSn, typically exhibit Curie−Weiss paramagnetic behavior at higher temperatures and antiferromagnetic behavior at lower temperatures, typically below 25 K. There are some exceptions, such as Eu_3P_2 and Eu_3As_2, which are both ferromagnetic semiconductors with Curie temperatures of 25 and 17.5 K, respectively.[34]

Herein we report the structural, magnetic, and electronic properties of a new compound, Eu_3InP_3, which was initially produced serendipitously while investigating the crystallization of compounds with the $Eu_{14}InP_{11}$ stoichiometry. Eu_3InP_3 is the first magnetic compound that is isostructural with Sr_3InP_3.[35] It exhibits several unusual low-temperature magnetic ordering transitions.

Experimental Section

Synthesis. Large $3 \times 1 \times 1$ mm^3 needle-shaped single crystals of Eu_3InP_3 are formed from a reaction of elemental Eu/P/In in the ratio of 14:11:551, where indium is both a reactant and the flux.[36] All reactants and products were handled under a nitrogen atmosphere. Europium metal of 99.999% purity, obtained in ribbon form from the Ames Laboratory, was cut into small pieces, and red phosphorus, obtained from J. Matthey or Puratronic, was ground to small grains with an agate mortar and pestle. The europium and phosphorus were packed into an alumina crucible between layers of granular indium metal of 99.99% purity obtained from Aesar. A second crucible containing quartz wool was inverted over the reaction crucible, and the entire reaction vessel was sealed in a fused silica jacket that was back-filled with argon at 0.2 atm.

The reaction sequence involved heating the vessel to 500 °C, holding for 1 h at 500 °C, heating to 1100 °C, holding for 6 h at 1100 °C, slow cooling at 3 °C/h to 850 °C, holding for 19 h at 850 °C, and then centrifuging at 850 °C. The elemental ratios of 1:1:40 and 1:1:30 for Eu/P/In were also investigated but resulted in a mixture of crystals of Eu_3InP_3 and a new phase identified as $Eu_3In_2P_4$ by single-crystal X-ray diffraction.

The reaction was also performed in sealed tantalum tubes, which were sealed in evacuated quartz ampules. Various reaction profiles were also investigated with the elements in the stoichiometric ratio of 3:1:3 for Eu/In/P. Dwell temperatures of 1100 and 1300 °C for periods of up to 6 days were employed in these preparations. The product from these reactions was identified as $Eu_{14}InP_{11}$ by X-ray diffraction.

All products were manipulated in a nitrogen-filled glovebox. The Eu_3InP_3 crystals are extremely reactive, decomposing into a yellow powder upon exposure to air.

X-ray Powder Diffraction. The Eu_3InP_3 products were ground in a drybox to a powder with an agate mortar and pestle and placed between pieces of cellophane tape with ∼10% of NBS silicon standard. The Eu_3InP_3 was transferred from the drybox to a Guinier camera, where the sample remained under vacuum for the duration of the data collection, which used Cu Kα1 radiation. Film data from the samples were compared to powder patterns calculated from the single-crystal structure of $Eu_{14}InP_{11}$ as well as from other known binary and ternary compounds. The powder diffraction pattern could be indexed according to the single-crystal structure of Eu_3InP_3, and no impurities were observed in the powder diffraction pattern.

Single-Crystal X-ray Diffraction. The Eu_3InP_3 crystals were stored in Exxon Paratone-N oil and transferred to the crystallography laboratory in dry ice. A suitable crystal of $0.28 \times 0.08 \times 0.02$ mm^3 volume was fixed to a glass fiber with silicon grease. A Siemens P3 diffractometer equipped with a modified Enraf−Nonius low-temperature apparatus and a graphite monochromator was used for data collection using Mo Kα radiation. The crystals were centered and indexed, and the ψ-scan method was used to perform an empirical absorption correction. The structure was solved by direct methods and refined by the full-matrix least-squares method

(14) Deakin, L.; Lam, R.; Marsiglio, F.; Mar, A. *J. Alloys Compd.* **2002**, *388*, 69−72.
(15) Johrendt, D.; Mewis, A.; Drescher, K.; Wasser, S.; Michels, G. *Z. Anorg. Allg. Chem.* **1996**, *1996*, 589−592.
(16) Payne, A. C.; Olmstead, M. M.; Kauzlarich, S. M.; Webb, D. J. *Chem. Mater.* **2001**, *13*, 1398−1406.
(17) Fisher, I. R.; Wiener, T. A.; Bud'ko, S. L.; Canfield, P. C.; Chan, J. Y.; Kauzlarich, S. M. *Phys. Rev. B: Solid State* **1999**, *59*, 13829−13834.
(18) Chan, J. Y.; Kauzlarich, S. M.; Klavins, P.; Liu, J.-Z.; Shelton, R. N.; Webb, D. J. *Phys. Rev. B: Solid State* **2000**, *61*, 459−463.
(19) Fisher, I. R.; Bud'ko, S. L.; Song, C.; Canfield, P. C.; Ozawa, T. C.; Kauzlarich, S. M. *Phys. Rev. Lett.* **2000**, *85*, 1120−1123.
(20) Holm, A. P.; Kauzlarich, S. M.; Morton, S. A.; Waddill, G. D.; Pickett, W. E.; Tobin, J. G. *J. Am. Chem. Soc.* **2002**, *124*, 9894−9898.
(21) Kauzlarich, S. M.; Payne, A. C.; Webb, D. J. Magnetism and Magnetotransport Properties of Transition Metal Zintl Isotypes. In *Magnetism: Molecules to Materials III*; Miller, J. S., Drillon, M., Eds.; Wiley-VCH: Weinheim, Germany, 2002; pp 37−62.
(22) Sánchez-Portal, D.; Martin, R. M.; Kauzlarich, S. M.; Pickett, W. E. *Phys. Rev. B: Solid State* **2002**, *65*, 144414.
(23) Kim, H.; Condron, C. L.; Holm, A. P.; Kauzlarich, S. M. *J. Am. Chem. Soc.* **2000**, *122*, 10720−10721.
(24) Kim, H.; Olmstead, M. M.; Chan, J. Y.; Canfield, P. C.; Fisher, I. R.; Henning, R. W.; Schultz, A. J.; Kauzlarich, S. M. *J. Solid State Chem.* **2001**, *157*, 225−232.
(25) Holm, A. P.; Olmstead, M. M.; Kauzlarich, S. M. *Inorg. Chem.* **2003**, *42*, 1973−1981.
(26) Badding, J. V.; Stacy, A. M. *Phys. Rev. B: Condens. Matter* **1987**, *35*, 8880−8883.
(27) Bauhofer, W.; Steigenberger, U.; Brown, P. J. *J. Magn. Magn. Mater.* **1987**, *67*, 49−54.
(28) Thalmeier, P. *J. Magn. Magn. Mater.* **1986**, *58*, 207−215.
(29) Bauhofer, W.; Chattopadhyay, T.; Moellendorf, M.; Gmelin, E.; Von Schnering, H. G.; Steigenberger, U.; Brown, P. J. *J. Magn. Magn. Mater.* **1986**, *54−57*, 1359−1360.
(30) Bauhofer, W.; Gmelin, E.; Moellendorf, M.; Nesper, R.; Von Schnering, H. G. *J. Phys. C: Solid State Phys.* **1985**, *18*, 3017−3035.
(31) Chattopadhyay, T.; Brown, P. J.; Thalmeier, P.; Von Schnering, H. G. *Phys. Rev. Lett.* **1986**, *57*, 372−375.
(32) Ernet, U.; Muellmann, R.; Mosel, B. D.; Eckert, H.; Poettgen, R.; Kotzyba, G. *J. Mater. Chem.* **1997**, *7*, 255−257.
(33) Chan, J. Y.; Rehr, A.; Webb, D. J.; Kauzlarich, S. M. *Chem. Mater.* **1997**, *9*, 2131−2138.
(34) Hulliger, F.; Vogt, O. *Solid State Commun.* **1970**, *8*, 771−772.
(35) Cordier, G.; Schäfer, H.; Stelter, M. *Z. Naturforsch.* **1987**, *42B*, 1268−1272.
(36) Canfield, P. C.; Fisk, Z. *Philos. Mag. B* **1992**, *65*, 1117−1123.

on F^2 (SHELXL-97, Sheldrick 1997). The structure was found to be isotypic with Sr_3InP_3.[35] The data were corrected for extinction and refined with anisotropic thermal parameters.

Conductivity Measurements. The resistance of Eu_3InP_3 is so high that it exceeds the measurement limit of our four-probe instrument over most of the temperature range between 10 and 300 K. Thus, a two-probe measurement method was employed in which, in a nitrogen-filled drybox, Pt leads were attached to the crystal with Epoxy Technology H20E-175 silver epoxy. The sample was protected in an airtight jar when taken out of the drybox and was exposed in air for about 10 s when being placed in the measurement chamber. Temperature-dependent conductivity was obtained on a single crystal with a $0.3 \times 0.1 \times 0.2$ mm^3 volume. The sample exhibited ohmic behavior. The measurement was reproduced on several different crystals. A Keithley model 617 programmable electrometer (200 GΩ limit) was used to measure the resistance. The current was selected automatically by the electrometer as the resistance of the sample changed to ensure measurement accuracy. The conductivity is calculated from the resistance measurement and the size of the crystal.

Magnetic Susceptibility Measurements. A Quantum Design MPMS superconducting quantum interference device (SQUID) magnetometer with a 7 T superconducting magnet was used to make dc magnetization measurements. A single crystal was placed in a drinking straw and secured with Paratone-N oil; several different crystals were studied. In addition, to ensure that the phase and crystallographic orientation were correct, single-crystal X-ray diffraction data were collected on a crystal after the magnetic measurements. The long axis of the crystal was confirmed to coincide with the *b*-axis of the unit cell. A powdered sample prepared from a number of crystals was also investigated. Zero field cooled data were collected from 2 to 300 K, and field cooled data were collected from 300 to 2 K. The data were collected utilizing the MultiVue software provided by Quantum Design.[37] Magnetization versus field data were obtained at fields up to 2 T at 2, 5, 8, 12, and 16 K.

Mössbauer Spectral Measurements. The europium-151 Mössbauer spectra were obtained on a constant-acceleration spectrometer that utilized a 151^mSmF_3 source. The absorber, which contained $\sim$60 mg/cm^2 of powdered sample mixed with boron nitride, was prepared and maintained under a dry nitrogen atmosphere. The spectra were measured in a Janis Super-Varitemp cryostat, and the temperature was controlled with a Lakeshore Cryogenics temperature controller with an accuracy of at least 1% of the observed temperature. The velocity scale was calibrated at room temperature with a cobalt-57 source and an α-iron foil. The isomer shifts are reported relative to EuF_3 at room temperature.

Heat Capacity. The heat capacity was measured on a Quantum Design physical property measurement system (PPMS) using a thermal relaxation method. The system utilizes a helium-3 refrigerator to reach temperatures below 2 K. Low-temperature data were obtained between 0.36 and 30 K on a 3.13 mg rectangular single crystal with applied magnetic fields of 0, 0.1, and 1 T. The crystal integrity was verified after the calorimetry measurement by magnetization. The Apiezon N-grease correction to the addenda for the heat capacity measurements was not applied to the field measurements, which may introduce an error as large as 1% in the sample heat capacity at temperatures below 10 K. Although the 0.1 T measurement may reflect a slight deviation from actual temperature values below 10 K due to the different thermometer calibration field factor utilized for this measurement, this deviation is negligible. The data points are extrapolated to zero temperature for the calculation of the entropy, which is obtained by integrating the specific heat divided by the temperature with respect to the temperature either from 0 to 30 K for the zero field or from 0 to 25 K for the applied field measurements.

(37) Quantum Design Inc., San Diego, CA 92121.

Results and Discussion

Synthesis. Molten metal fluxes have been used to grow large single crystals for the characterization of physical properties.[36,38] Indium is an ideal flux because of its low melting point, relative inertness to the alumina reaction crucible, minimal wetting effects, and low vapor pressure. An indium flux was originally employed in an attempt to prepare large crystals of $Eu_{14}MnP_{11}$. Although this proved to be unsuccessful, a new compound, Eu_3InP_3, was obtained. This compound cannot be prepared from a stoichiometric mixture of the three elements sealed in tantalum tubes at the temperatures investigated. This suggests that the phase is peritectic or that competing thermodynamic phases are more stable. It is possible that Eu_3InP_3 is a kinetic product that results when large amounts of indium are present.

Structure. Ternary Zintl compounds with the 3:1:3 stoichiometry typically crystallize in one of three structure-types, two of which are orthorhombic with the *Pnma* space group[39,40] and the third of which is monoclinic with the *Cmca* space group.[39] All three structure-types possess chains of MPn_4 tetrahedra, but they differ in the connectivity of these tetrahedra. Eu_3InP_3 is isotypic with Ca_3InP_3,[40] Sr_3InP_3,[35] and Ca_3GaAs_3,[40] all of which are composed of distorted $[MPn_2Pn_{2/2}]^{6-}$ tetrahedra (where M is Ga or In and Pn is P or As) that are corner-shared to form linear chains. Because two of the Pn ions are shared by two tetrahedra, these two Pn ions are denoted as $Pn_{2/2}$ in the above formulation. The heavier antimony-containing compounds, Sr_3GaSb_3 and Ba_3GaSb_3, have structural motifs based on chains of tetrahedra as well. Sr_3GaSb_3 has nonlinear chains of corner-shared $[GaSb_2Sb_{2/2}]^{6-}$ tetrahedra.[35] Large cations, in conjunction with antimony, result in compounds with the Ba_3GaSb_3 structure which contains isolated $[Ga_2Sb_6]^{12-}$ dimers composed of edge-shared tetrahedra.[40] In each of the structure-types, the tetrahedral angles are distorted from the ideal values.

Each of the aforementioned structures can be rationalized with the Zintl concept.[35,40] The net charge of the Eu_3InP_3 formula unit is zero when europium is divalent such that the compound may be formulated as containing three Eu^{2+}, one In^{3+}, and three P^{3-} ions. Alternatively, the Zintl electron counting scheme yields $(Eu^{2+})_3(4bIn^-)(2bP^-)(1bP^{2-})_2$ where *b* indicates the number of bonds to each element. Thus, formally, the In and P ions combine to form a polyanion, $[InP_2P_{2/2}]^{6-}$, which counterbalances the charge of the three Eu^{2+} cations.

(38) Fisk, Z.; Remeika, J. P. Growth of Single Crystals from Molten Metal Fluxes. In *Handbook on the Physics and Chemistry of Rare Earths*; Gschneidner, K. A., Eyring, L., Eds.; Elsevier Science B.V.: Amsterdam, Netherlands, 1989; Vol. 12, p 53.

(39) Cordier, G.; Savelsberg, G.; Schäfer, H. *Z. Naturforsch.* **1982**, *37B*, 975−980.

(40) Cordier, G.; Schäfer, H.; Stelter, M. *Z. Naturforsch.* **1985**, *40B*, 1100−1104.

Table 1. Selected Crystallographic Data for Eu_3InP_3

temp/K	140(2)
wavelength/Å	0.71073
cryst system, space group, *Z*	orthorhombic, *Pnma*, 4
unit cell dimensions/Å	$a = 12.6517(15)$
	$b = 4.2683(5)$
$\alpha = \beta = \gamma = 90°$	$c = 13.5643(14)$
vol/Å^3	732.49(14)
D_c/(g cm^{-3})	6.018
μ/mm^{-1}	28.975
reflns collected	4769
observed reflns ($I > 2\sigma(I)$)	160
data/restraints/params	1365/0/44
S (goodness-of-fit on F^2)	1.051
final *R* indices [I > 2σ(I)]	R1[a] = 0.0370, wR2[b] = 0.0946
R indices (all data)	R1 = 0.0404, wR2 = 0.0971
extinction coeff	0.0027(3)
largest diff. peak and hole/(e Å^{-3})	3.338 and −3.812

[a] $R1 = \sum||F_o| - |F_c||/\sum|F_o|$. [b] $wR2 = [\sum[w(F_o^2 - F_c^2)^2]/\sum[w(F_o^2)^2]]^{1/2}$.

Table 2. Selected Bond Lengths [Å] and Angles [deg] for Eu_3InP_3[a]

Eu(1)−P(1)#1	2.974(2)	P(1)#2−Eu(1)−In#1	104.68(5)
Eu(1)−P(3)	2.991(2)	P(3)−Eu(1)−In#1	138.28(2)
Eu(1)−P(2)#2	3.109(2)	P(2)#2−Eu(1)−In#1	102.16(4)
Eu(1)−In#1	3.3236(7)	P(2)#1−Eu(1)−In#1	47.87(4)
Eu(1)−Eu(2)#3	3.5954(7)	In#1−Eu(1)−In#2	79.90(2)
Eu(1)−Eu(3)#4	3.9052(6)	Eu(2)#3−Eu(1)−Eu(3)#4	102.61(2)
Eu(1)−Eu(2)	4.0235(8)	Eu(3)#4−Eu(1)−Eu(3)#9	66.253(12)
Eu(1)−Eu(3)	4.0851(7)	Eu(2)#3−Eu(1)−Eu(2)	154.34(2)
Eu(2)−P(1)	2.989(2)	Eu(3)#4−Eu(1)−Eu(2)	98.819(13)
Eu(2)−P(1)#2	3.027(2)	Eu(2)#3−Eu(1)−Eu(3)	59.470(13)
Eu(2)−P(2)#5	3.166(2)	Eu(3)#4−Eu(1)−Eu(3)	143.836(8)
Eu(2)−P(3)#6	3.423(2)	Eu(2)−Eu(1)−Eu(3)	94.868(14)
Eu(2)−In#2	3.7255(7)	P(1)−Eu(2)−P(1)#2	95.52(6)
Eu(2)−Eu(3)#6	3.8331(8)	P(1)#2−Eu(2)−P(1)#1	89.67(7)
Eu(2)−Eu(2)#1	4.0445(8)	P(1)−Eu(2)−P(2)#5	91.46(6)
Eu(3)−P(1)#3	3.644(2)	P(1)#2−Eu(2)−P(2)#5	172.53(6)
Eu(3)−P(2)#1	3.001(2)	P(1)#1−Eu(2)−P(2)#5	92.35(5)
Eu(3)−P(3)#6	3.076(2)	P(1)−Eu(2)−P(2)#10	91.46(6)
Eu(3)−P(3)#7	3.155(2)	P(2)#5−Eu(2)−P(2)#10	84.77(6)
Eu(3)−In#1	3.6259(7)	P(1)−Eu(2)−P(3)#6	179.85(7)
Eu(3)−In#8	3.7145(8)	P(1)#2−Eu(2)−P(3)#6	84.38(5)
In−P(1)	2.585(2)	P(2)#5−Eu(2)−P(3)#6	88.66(5)
In−P(3)#9	2.598(2)	P(2)#1−Eu(3)−P(2)#2	90.64(6)
In−P(2)	2.617(2)	P(2)#1−Eu(3)−P(3)#6	88.85(6)
		P(2)#1−Eu(3)−P(3)#7	175.79(5)
P(1)#1−Eu(1)−P(1)#2	91.71(7)	P(2)#2−Eu(3)−P(3)#7	92.02(4)
P(1)#1−Eu(1)−P(3)	114.19(6)	P(3)#6−Eu(3)−P(3)#7	94.46(5)
P(1)#1−Eu(1)−P(2)#2	146.77(7)	P(1)−In−P(3)#9	113.80(6)
P(1)#2−Eu(1)−P(2)#2	81.45(5)	P(3)#9−In−P(3)#4	110.46(9)
P(3)−Eu(1)−P(2)#2	98.11(6)	P(1)−In−P(2)	99.49(8)
P(2)#2−Eu(1)−P(2)#1	86.70(6)	P(3)#9−In−P(2)	109.32(6)
P(1)#1−Eu(1)−In#1	48.07(5)	In#7−P(3)−In#11	110.46(9)

[a] Symmetry transformations used to generate equivalent atoms: (#1) $-x + 1, -y + 1, -z + 1$; (#2) $-x + 1, -y, -z + 1$; (#3) $x - 1/2, y, -z + 1/2$; (#4) $-x + 1/2, -y + 1, z + 1/2$; (#5) $-x + 3/2, -y + 1, z - 1/2$; (#6) $x + 1/2, y, -z + 1/2$; (#7) $-x + 1/2, -y, z - 1/2$; (#8) $x, y, z-1$; (#9) $-x + 1/2, -y, z + 1/2$; (#10) $-x + 3/2, -y, z - 1/2$; (#11) $-x + 1/2, -y + 1, z - 1/2$.

Eu_3InP_3 crystallizes in the orthorhombic *Pnma* space group. The crystals grow with a needle shape, with the needle axis parallel to the [010] direction. Table 1 gives the crystallographic data collection parameters and details of the structure solution and refinement. Selected distances and angles are given in Table 2. Figure 1 shows the anionic building block of the Eu_3InP_3 structure, that is, the one-dimensional chains of corner-shared $[InP_2P_{2/2}]^{6-}$ tetrahedra isolated by the divalent europium ions.

Figure 2 identifies the atoms in Eu_3InP_3 by the numbering scheme in Table 2 and shows the anisotropic displacement ellipsoids at the 90% probability level. The local environments of indium and europium in Eu_3InP_3 are also shown in Figure 2. The $[InP_2P_{2/2}]^{6-}$ tetrahedra share the P(3) site.[35,40] The In−P bond distances, which range from 2.585(2) to 2.617(2) Å, are similar to those found in Ca_3InP_3 and Sr_3InP_3. The $[InP_2P_{2/2}]^{6-}$ tetrahedra are distorted with P−In−P bond angles of 99.49(8), 109.23(6), 110.46(9), and 113.80(6)°; the smallest angle is formed by P(1)−In−P(2). These angles are similar to those observed in Sr_3InP_3 and Ca_3InP_3.[35,40] The long axis of the chain is aligned parallel to the [010] orientation. Eu(1) is surrounded by five phosphorus ions with distances ranging from 2.974(2) to 3.109(2) Å, yielding a distorted square pyramidal coordination environment. These square pyramids share edges with each other to form Eu(1) chains along the *b*-axis. The distance of 2.974(2) Å is quite short for a Eu−P distance. Eu(2) is in the center of a distorted octahedron made up of six P ions. The Eu(2)−P distances range from a set of five between 2.989(2) and 3.166(2) Å to a sixth at 3.423(2) Å. The octahedra share P(1)−P(2) edges to form chains parallel to [010]; two of these chains are joined together through a sharing of P(1)−P(1) edges. Eu(3) is in a coordination environment that is similar to that of Eu(2), but its octahedral

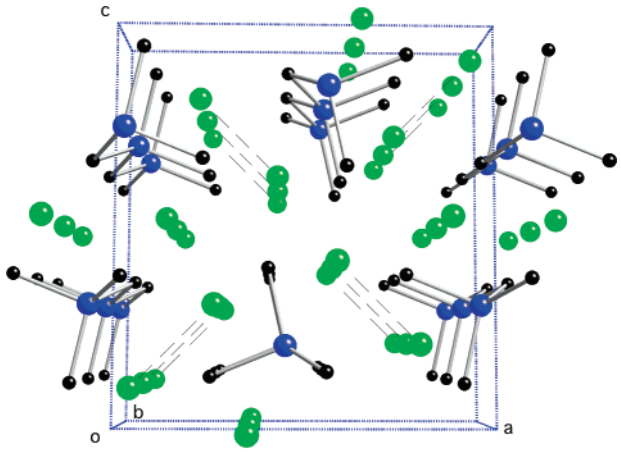

Figure 1. Perspective view down the *b*-axis of the unit cell of Eu_3InP_3. The Eu, In, and P atoms are shown in green, blue, and black, respectively. Dashed lines show the short Eu−Eu distance.

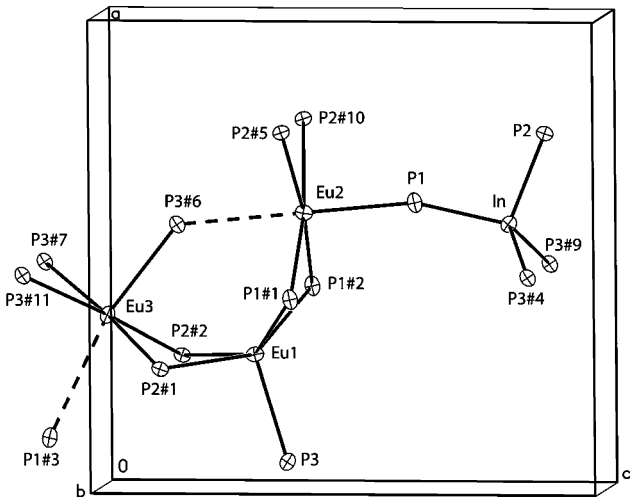

Figure 2. Partial structure of Eu_3InP_3 showing the numbering scheme and the local europium and indium environments. The anisotropic displacement ellipsoids are shown at the 90% probability level.

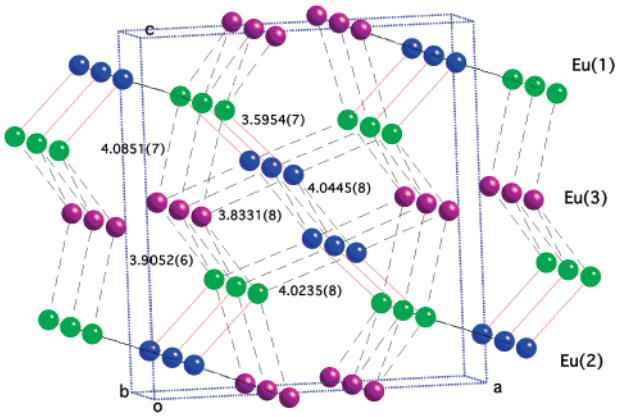

Figure 3. Lattice structure of the europium sites in Eu_3InP_3. Eu(1), Eu(2), and Eu(3) are shown in green, blue, and purple, respectively. The shortest Eu−Eu distance is shown by the solid red lines.

environment is more distorted with five distances ranging from 3.001(2) to 3.155(2) Å and a sixth at 3.644(2) Å. The shorter Eu−P distances in Eu_3InP_3, ranging from 2.974(2) to 3.166(2) Å, are consistent with the Eu−P distances observed in binary europium phosphides, such as EuP_7, Eu_3P_4, and EuP.[41] This indicates the presence of covalent interactions between Eu and P.[41]

The Eu−Eu distances in Eu_3InP_3 range from 3.5954(7) to 4.0851(7) Å. Figure 1 illustrates the shortest Eu−Eu distance of 3.5954(7) Å with dashed lines. This is much smaller than the 3.967 Å distance observed in europium metal. The Eu-only lattice, along with distances, is shown in Figure 3, where the closest Eu−Eu distances are indicated by solid lines. However, aside from the one short distance of 3.5954(7) Å, the others are very similar and vary by about 0.2 Å. The europium ions form triangles with edge distances of 3.5954(7), 3.8331(8), and 4.0851(7) Å. These triangles further build up a 3D network with pentagonal tunnels in which the $[InP_2P_{2/2}]_n^{6n-}$ chains reside. Also, there is a zigzag chain along the *b*-axis, indicated by dotted lines with a distance of 3.9052(6) Å. The Eu(1) repeat distance is dictated by the *b*-axis dimension and is relatively long at 4.2683(5) Å.

Conductivity. The conductivity of Eu_3InP_3 as a function of temperature is shown in Figure 4. Because the conductivity below 80 K is too low to be measured, its temperature dependence could only be obtained above 80 K. The temperature dependence of the conductivity indicates that Eu_3InP_3 is a semiconductor with a room-temperature conductivity of 5.84(12) S/m. A plot of ln σ as a function of the inverse temperature is shown in the inset to Figure 4. By using the relationship

$$\ln \sigma = F - (E_g/2k_BT)$$

a gap energy, E_g, of 0.454(3) eV is obtained.

Magnetic Susceptibility Studies. Figure 5 shows the temperature dependence of magnetic susceptibility of Eu_3InP_3 measured in a field of 0.010 T on a needle-shaped single crystal whose long needle *b*-axis was parallel with

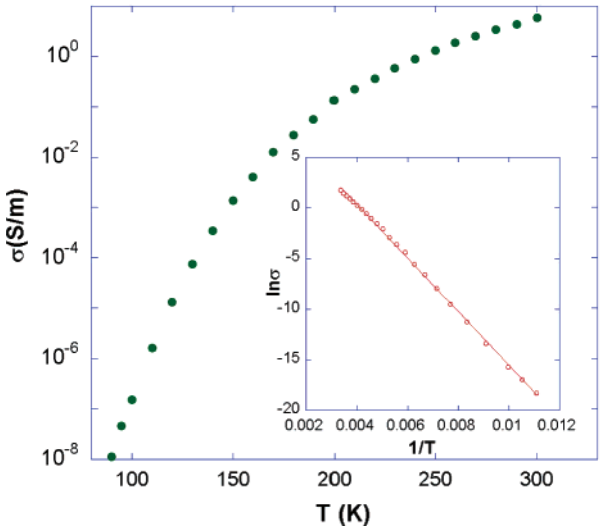

Figure 4. Conductivity of Eu_3InP_3 as a function of temperature. The inset shows the fit of the data with the expression given in the text.

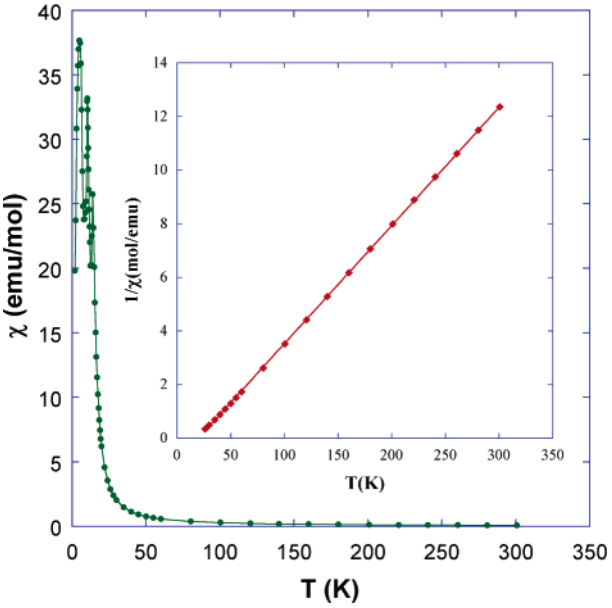

Figure 5. Single-crystal molar magnetic susceptibility of Eu_3InP_3 as a function of temperature obtained with the *b*-axis aligned parallel to an applied magnetic field of 0.010 T. The inset shows a Curie−Weiss fit to the inverse molar magnetic susceptibility obtained between 26 and 300 K.

the applied magnetic field. The magnetic susceptibility can be fit with the Curie−Weiss law

$$\chi = C/(T - \theta)$$

over the temperature range of 26 to 300 K, and it yields a Curie constant, *C*, of 22.70(4) (emu K)/mol and a Weiss temperature, θ, of 19.9(3) K. The effective magnetic moment, μ_{eff}, calculated from the Curie constant is 13.47(1) μ_B, a moment that is close to the 13.75 μ_B value expected for three divalent europium ions. Below 15 K, several magnetic transitions are observed in Eu_3InP_3. More specifically, three peaks appear at 14, 10.4, and ~5 indicating complex magnetic interactions.

To obtain more information about these three magnetic transitions, zero field cooled (ZFC) and field cooled (FC)

(41) Hulliger, F. Rare Earth Pnictides. In *Handbook on the Physics and Chemistry of Rare Earths*; Gshneidner, K. A., Eyring, L., Eds.; Elsevier/North Holland, Inc.: New York, 1979; Vol. 4, pp 153−236.

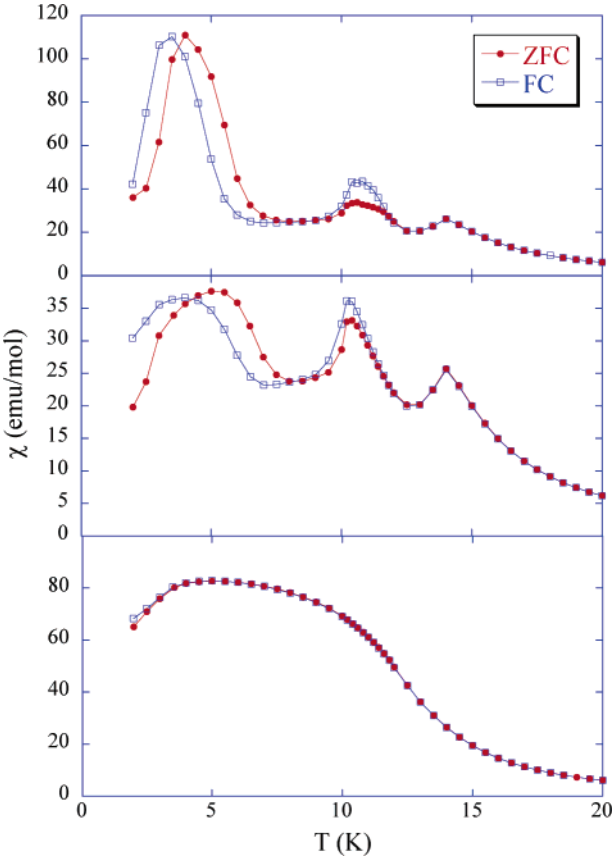

Figure 6. Zero field and field cooled single-crystal molar magnetic susceptibility of Eu_3InP_3 as a function of temperature obtained with the *b*-axis aligned parallel to the applied magnetic field. The field strengths from top to bottom are 0.001, 0.010, and 0.100 T, respectively.

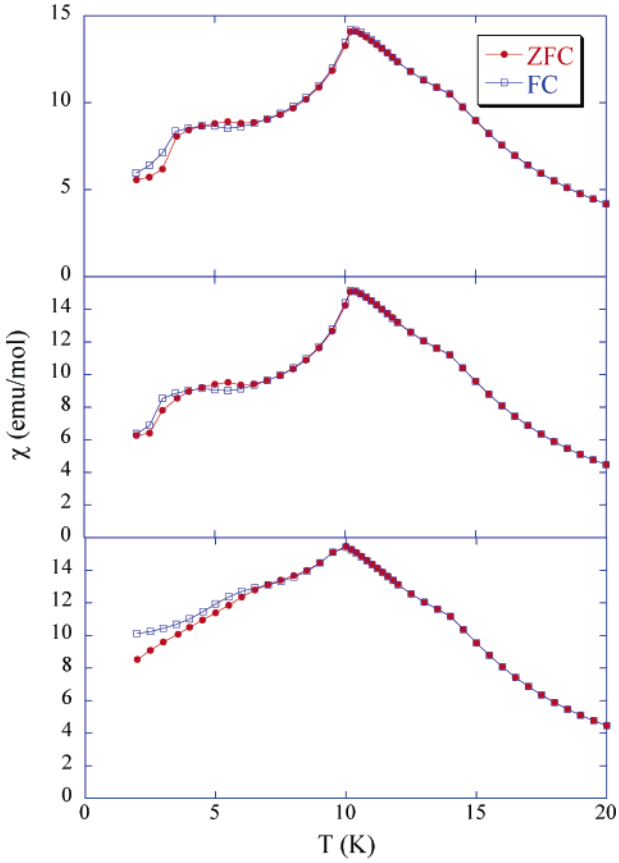

Figure 7. Zero field and field cooled single-crystal molar magnetic susceptibility of Eu_3InP_3 as a function of temperature obtained with the *b*-axis aligned perpendicular to the applied magnetic field. The field strengths from top to bottom are 0.001, 0.010, and 0.100 T, respectively.

susceptibilities were collected at different applied magnetic fields between 2 and 20 K. Figure 6 shows the magnetic susceptibility of a crystal of Eu_3InP_3 with its *b*-axis oriented parallel to the applied field. At an applied field of 0.001 T, the ZFC and FC susceptibilities are identical between 300 and 13 K. Below 13 K, they diverge and intersect with each other twice at ~8.5 and 4 K. This behavior suggests the presence of a ferromagnetic or canted antiferromagnetic interaction below 13 K. The magnetic susceptibility obtained at 0.010 T is very similar to that obtained at 0.001 T, but the peaks in the susceptibility at 10.4 and 5 K are suppressed. Further, the temperatures of the susceptibility maxima shift compared with the 0.001 T data. More specifically, the 10.4 K susceptibility maximum moves to a lower temperature and the 5 K susceptibility maximum moves to a higher temperature. At 0.100 T, all the peaks are suppressed except for a small ZFC and FC divergence below 4 K. Figure 7 shows the same measurements as those in Figure 6 except that the field is applied perpendicular to the *b*-axis of the crystal. The results shown in Figure 7 are quite different from those in Figure 6, indicating the anisotropic nature of the magnetic transitions in Eu_3InP_3. Isotropically shaped crystals were also investigated and yielded the same results. In Figure 7, there are two obvious antiferromagnetic transitions at 10.4 and 14 K, consistent with the transitions observed with the field applied parallel to the *b*-axis; these peaks in the susceptibility are not suppressed even at an applied field of 0.100 T.

The crossing of the ZFC and FC susceptibilities observed below 8 K in Figure 6 suggests the presence of either complex magnetic interactions or domain motions in Eu_3InP_3. To investigate whether the magnetic transitions observed in Eu_3InP_3 are caused by domain wall motion within the single-crystal sample, ZFC and FC data were obtained on a powder sample of Eu_3InP_3. Grinding the sample into a very fine powder may disrupt the domain boundaries and thus decrease the domain effects. The results of this study, shown in Figure 8, indicate that the intersections of the susceptibility disappear and that the temperature dependence becomes simpler. This result supports the hypothesis that domain wall motion effects produce the complex transitions in the magnetic susceptibility below 8 K. However, because the complex behavior is observed mainly in the *b*-axis parallel direction, it is also possible that information is lost by averaging the various directions obtained in a powdered sample.

Heat capacity results, which will be discussed below, also indicate that the 5 K transition is an intrinsic magnetic transition. There are two reasons: first, there is a shoulder from 2 to 8 K in the heat capacity curve, and, second, the heat capacity curve measured between 2 and 8 K in a 1 T applied field is quite different from that obtained in the absence of a field.

Europium-151 Mössbauer Spectral Studies. The europium-151 Mössbauer spectra of Eu_3InP_3, obtained between 4.2 and 90 K, are shown in Figure 9. At 90 K, two absorption

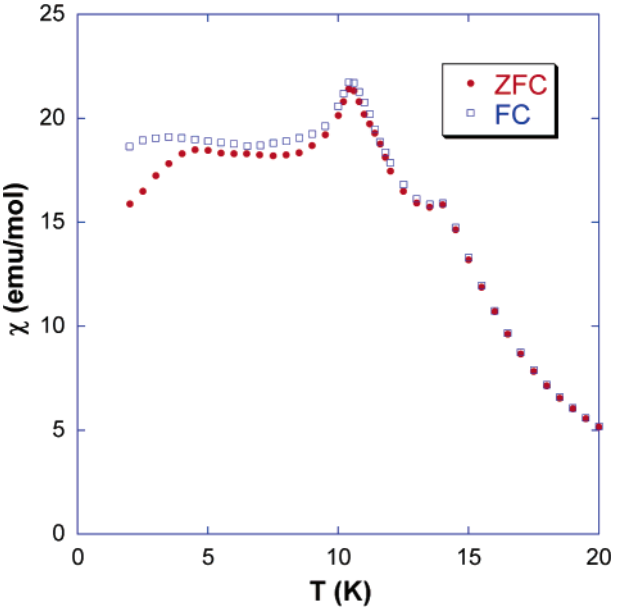

Figure 8. Temperature dependence of the magnetic susceptibility observed for a powdered sample of Eu_3InP_3 obtained in a 0.010 T applied magnetic field.

regions are observed in the spectra: a major component at ~ -10 mm/s and a minor component at ~ 1 mm/s. The five spectra have been fit simultaneously to ensure a consistent temperature dependence of the hyperfine parameters.

The minor spectral component, which has a relative area of 5% and an isomer shift of 1 mm/s, has been constrained to be independent of temperature. This isomer shift is characteristic of europium(III) and indicates a small oxidation of the sample, perhaps on the surface of the particles. This minor absorption, which is a singlet at all temperatures, is assigned to an unknown europium(III) oxidation impurity that is not intrinsic to Eu_3InP_3.

The major spectral component at ~ -10 mm/s indicates that europium is present as divalent europium in Eu_3InP_3. At 90 K, this spectral component is a broad singlet characteristic of paramagnetic europium(II), whereas, at 16 K, this component exhibits the onset of magnetic ordering of some of the europium(II) ions. In contrast, at 12, 8, and 4.2 K, the spectra clearly exhibit magnetic ordering of some or all of the europium(II) sites.

The major spectral absorption observed in Eu_3InP_3 has been fit with three components with the same area assigned to the three crystallographically inequivalent europium sites. The line widths and the isomer shifts of these components have been fit but constrained to be independent of temperature. Because Eu_3InP_3 is paramagnetic at 90 K, as is indicated by the magnetic susceptibility measurements shown above, the 90 K spectrum has been fit with three singlets. Between 16 and 4.2 K, the spectra have been fit with three octets whose hyperfine fields have been varied. The resulting spectral hyperfine parameters are given in Table 3.

Because all three europium sites in Eu_3InP_3 have the same crystallographic degeneracies and rather similar environments, it is difficult to make an unambiguous assignment of the three Mössbauer spectral components to the three

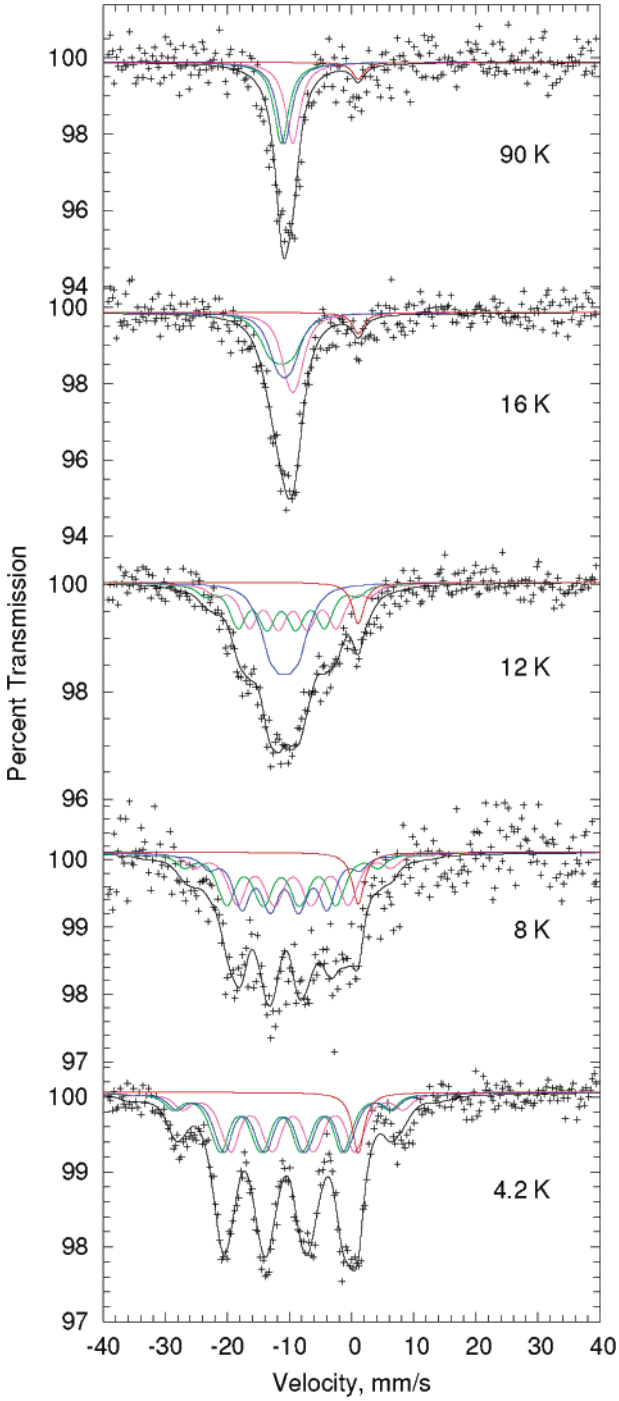

Figure 9. Europium-151 Mössbauer spectra of Eu_3InP_3 obtained at the indicated temperatures.

crystallographic europium(II) sites. The following tentative assignment (see Table 3) is proposed on the basis of the Wigner−Seitz cell volumes and the Eu−Eu average bond distances for the three crystallographically distinct europium sites. A Wigner−Seitz cell analysis,[42] which has been carried out with the 12-coordinate metallic radii of 1.99, 1.61, and 1.28 Å for Eu, In, and P, respectively, yields volumes of 40.561, 42.124, and 41.310 $Å^3$ for the Eu(1), Eu(2), and Eu(3) sites, respectively. The Eu−Eu average bond distances, obtained from the distances given in Table 2 for the near-

(42) Gelato, L. *J. Appl. Crystallogr.* **1981**, *14*, 151−153.

Table 3. Europium-151 Mössbauer Spectral Hyperfine Parameters for Eu_3InP_3

T, K	$\delta_{Eu(1)}$, m/s	$H_{Eu(1)}$, T	$\delta_{Eu(2)}$,[a] mm/s	$H_{Eu(2)}$, T	$\delta_{Eu(3)}$,[a] mm/s	$H_{Eu(3)}$, T	Γ, mm/s	area, (%ϵ)/(mm/s)
90	−9.5(1)	0	−11.3(1)	0	−10.8(1)	0	2.9(2)	−30(1)
16	−9.5(1)	2(1)	−11.3(1)	5(1)	−10.8(1)	3(1)	2.9(2)	−38(1)
12	−9.5(1)	17.1(5)	−11.3(1)	17.0(5)	−10.8(1)	5.9(4)	2.9(2)	−53(1)
8	−9.5(1)	21.9(4)	−11.3(1)	21.5(5)	−10.8(1)	16.7(5)	2.9(2)	−53(1)
4.2	−9.5(1)	24.5(5)	−11.3(1)	24(1)	−10.8(1)	24(1)	2.9(2)	−56(1)

[a] The isomer shifts are given relative to room-temperature EuF_3.

neighbors as defined by the Wigner−Seitz cells, are 3.982, 4.011, and 4.091 Å for the Eu(1), Eu(2), and Eu(3), respectively. The Eu(1) site, which has the smallest Wigner−Seitz cell volume and the shortest Eu−Eu average bond distance, is characterized[43] by the least negative isomer shift. The Eu(2) site, which has the largest Wigner−Seitz cell volume, has the most negative isomer shift. The third component, with an intermediate isomer shift, is assigned to Eu(3), which has an intermediate Wigner−Seitz cell volume.

At 16 K, only small hyperfine fields of between 2 and 5 T are observed in Eu_3InP_3; these fields may result from short-range magnetic ordering slightly above the ordering temperature of 14 K. At 12 K, the Eu(1) and Eu(2) sites exhibit substantial fields of ~17 T. Eu(1) is expected to order antiferromagnetically at the highest temperature, because of its short Eu−Eu average bond distance and because it forms dimers (see above) with the Eu(2) site, which also exhibits a substantial hyperfine field.

The Eu(3) site experiences a small transferred field at 12 K and is magnetically ordered only at 8 and 4.2 K. This Eu(3) site may experience some magnetic frustration resulting from the antiferromagnetic coupling of the Eu(1) and Eu(2) sites in the triangular arrangement of the three europium sites (see Figure 3). The existence of frustration would be compatible with the indication of ferromagnetic or ferrimagnetic interactions in the divergence between the zero field cooled and field cooled magnetic susceptibilities (see Figure 6).

Because the Mössbauer spectral experiments have been carried out in zero applied field, there may be some differences in the magnetic transition temperatures observed in the Mössbauer and the magnetic experiments. The magnetic transition observed at 14 K in Figure 4 may be associated with the ordering of the Eu(1) and Eu(2) sites observed in the 12 K Mössbauer spectrum, and the transition observed at 10.4 K in Figure 4 may be associated with the ordering of all three europium(II) sites in the Mössbauer spectra obtained at 8 K. The application of a magnetic field of 0.001 T may decrease the transition temperatures by up to 2 K—it should be noted that the peak at 10 K in Figure 6 shifts to a lower temperature in an applied field of 0.010 T.

Heat Capacity. Figure 10 shows C_p/T, normalized per mole of europium, as a function of temperature under different applied magnetic fields. The lattice contribution, which increases with temperature monotonically at low

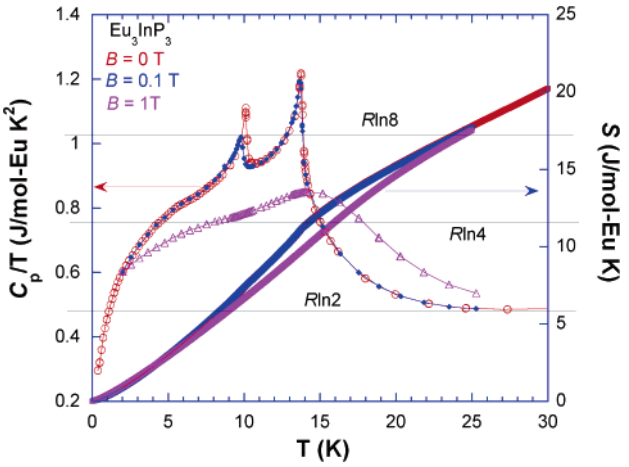

Figure 10. C_p/T and S versus temperature for Eu_3InP_3 obtained at the indicated applied magnetic fields.

temperature, will be small so that we can attribute the nonmonotonic behavior of C_p/T versus temperature to the magnetic contribution to the heat capacity. There are two obvious peaks at about 13.5 and 10 K, consistent with the two magnetic ordering transitions at 14 and 10.4 K observed in the magnetic susceptibility. These two transitions suggest that the interaction between the different divalent europium ions, the intersite interaction, may be weak, whereas the intrasite interaction is strong so that the crystallographically different sites order independently, as the Mössbauer spectral results indicate. The long tail above the 14 K transition temperature indicates the development of a short range order, which is also observed in the Mössbauer spectra. The ordering temperatures for both the 14 and 10.4 K transitions decrease in a 0.100 T applied field, although this decrease is very small for the 14 K transition. This is consistent with antiferromagnetic ordering at both transitions and suggests the possibility of a metamagnetic transition at a high magnetic field, which is clearly shown in the magnetization with respect to field data in Figure 11. The C_p/T values obtained in a 1 T applied field show a broad peak near 14 K, which is consistent with a ferromagnetic transition in the applied field. Because the paramagnetic spins will be already partially aligned in this applied field, the transition is not as sharp as in the zero field and low field data. The corresponding entropy is shown as the solid lines in Figure 10. The Eu^{2+} ground state, which is spherically symmetric, is weakly affected by the crystal field. Therefore, it is a reasonable approximation to consider the crystal field ground state as 8-fold degenerate. The entropy at 25 K, ~R ln 8 per mole of europium, where R is the gas constant, indicates that this 8-fold degenerate europium state is consistent with the magnetic susceptibility results. As the temperature is

(43) Holm, A. P.; Park, S.-M.; Condron, C. L.; Olmstead, M. M.; Kim, H.; Klavins, P.; Grandjean, F.; Hermann, R. P.; Long, G. J.; Kanatzidis, M. G.; Kauzlarich, S. M.; Kim, S.-J. *Inorg. Chem.* **2003**, *42*, 4660−4667.

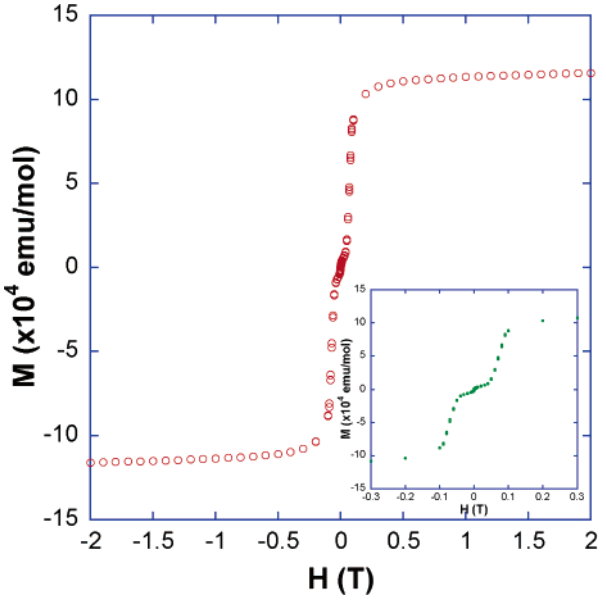

Figure 11. Single-crystal magnetization of Eu_3InP_3 measured at 5 K with the *b*-axis aligned parallel to the applied field. The inset is an enlargement of the magnetization obtained between ±0.3 T.

lowered below the transition temperature, the 8-fold degenerate state is depopulated through the magnetic ordering and entropy decreases. The total integrated entropy up through the 14 K transition is $2R$ ln 8. The missing R ln 8 entropy expected from the full ordering of the three europium ions per formula unit is contained in the fluctuations above 14 K and is not fully developed until about 25 K, an observation that is consistent with the Curie−Weiss temperature. Also consistent with this is the saturation magnetization at 5 K shown in Figure 11, where the full $gJ_z\mu_B = 7\ \mu_B$ per Eu ion develops. There exists approximately R ln 8 total entropy per mole at 8 K at the lower transition, indicating that there is still an 8-fold degeneracy present below the two transitions. This remaining degeneracy is lost in the broad hill-like feature in C_p/T. Zeeman splitting of magnetic levels due to strong internal molecular fields could possibly explain the shape of this feature. Similar behavior has been reported in some Gd compounds, such as $GdBa_2Cu_3O_7$ and Gd_2CuO_4.[44,45]

Magnetization Studies. Hysteresis curves have been measured, and the magnetization as a function of the field at 5 K obtained with the single crystal *b*-axis of Eu_3InP_3 parallel to the applied field is shown in Figure 11. The analogous perpendicular magnetization results are available in the Supporting Information. In the perpendicular direction, the magnetization increases linearly below 0.2 T, whereas above 0.2 T it starts to saturate. The parallel curve saturates at 1 T with a saturation moment of 20.777(8) μ_B per formula, which is consistent with the 21 μ_B expected for the three Eu^{2+} ions. The inset to Figure 11 shows the magnetization obtained between ±0.3 T. The sharp magnetization increase with the applied field between 0.05 and 0.1 T suggests a spin-flip transition. This is consistent with the heat capacity measurements (see Figure 10) which reveal that the observed C_p/T is very different when measured at 0 and 0.1 T versus at 1 T.

The parallel-direction magnetization obtained at 2, 8, 10, and 12 K is similar to the 5 K results shown in Figure 11. At high temperature, the magnetization is harder to saturate than at low temperature. At 16 K, which is above the magnetic transition temperature, the magnetization is linear up to ∼0.3 T and then begins to saturate. This can be explained by a local magnetic correlation between magnetic sites above the long range ordering temperature that is observed in the Mössbauer spectrum obtained at 16 K. Further, because the Weiss temperature, θ, obtained from the Curie−Weiss fit is positive, this correlation is believed to be ferromagnetic.

Because Eu_3InP_3 is a semiconductor, two possible mechanisms may explain the magnetic transitions: super-exchange and spin−spin exchange. However, super-exchange is expected to be minimal because, although the Eu−P bonds may have a strong covalent character, the f-orbitals of europium contribute very little to the bonding. Hence, spin−spin exchange is expected to be the dominant exchange interaction in Eu_3InP_3. Figure 3 shows the europium lattice along with some of the Eu−Eu distances. The shortest distance of 3.5954(7) Å is expected to provide the strongest interaction. All other distances are quite similar, ranging from 3.833 to 4.086 Å, and the interactions are expected to be much weaker. If Eu(1) and Eu(2) order antiferromagnetically first, as indicated by the Mössbauer spectral measurements, then one might expect complex or "frustrated" magnetic behavior for Eu(3) based on the triangular arrangement of the three divalent europium ions.

Summary. Eu_3InP_3 is a magnetic, semiconducting Zintl compound. There are three different Eu^{2+} sites, which interact in a complex fashion. Magnetic susceptibility, Mössbauer, and heat capacity studies indicate that there are three magnetic transitions at 14 K, 10.2 K, and ∼5 K. A spin-flip transition can be seen in the magnetization curve at 5 K with an applied field of 0.05 T.

Acknowledgment. The authors thank Prof. Alan F. Williams of the University of Geneva, for the use of the SmF_3 source, and Prof. Kai Liu, University of California−Davis, for useful discussions. The authors acknowledge the NSF (DMR-0120990, DMR-0433560) for financial support. F.G. acknowledges with thanks the financial support of the Fonds National de la Recherche Scientifique, Belgium, through Grant No. 9.456595 and a travel grant, and the Fonds de la Recherche Fondamentale Collective, Belgium, through Grant No. 2.4522.01.

Supporting Information Available: Crystallographic data is provided in CIF format. The perpendicular-direction magnetization curve measurement is provided in PDF format. This material is available free of charge via the Internet at http://pubs.acs.org.

IC048507O

(44) Brown, S. E.; Thompson, J. D.; Willis, J. O.; Aikin, R. M.; Zirngiebl, E.; Smith, J. L.; Fisk, Z.; Schwarz, R. B. *Phys. Rev. B: Condens. Matter* **1987**, *36*, 2298−2300.

(45) Thompson, J. D.; Cheong, S. W.; Brown, S. E.; Fisk, Z.; Oseroff, S. B.; Tovar, M.; Vier, D. C.; Schultz, S. *Phys. Rev. B: Condens. Matter* **1989**, *39*, 6660−6666.